Spectroscopic, Structural and Transport Properties of Conductive Polyaniline Processed from Fluorinated Alcohols

Patrice Rannou,* Anna Gawlicka, Detlef Berner, Adam Pron, and Maxime Nechtschein

Laboratoire de Physique des Métaux Synthétiques, UMR 5819 (CEA-CNRS−Université J. Fourier Grenoble I), Département de Recherche Fondamentale sur la Matière Condensée, CEA-Grenoble, 17 Rue des Martyrs, 38 054 Grenoble Cedex 9, France

David Djurado

Laboratoire de Spectrométrie Physique, UMR 5588 (CNRS−Université J. Fourier Grenoble I), BP 87, 38 402 St Martin d'Hères Cedex, France

Received September 16, 1997; Revised Manuscript Received February 13, 1998

ABSTRACT: Studies of PANI protonation in fluorinated alcohols are presented. Three solvents have been tested, namely 1,1,1,3,3,3-hexafluoro-2-propanol (HFIP), 1,1,1,3,3,3-hexafluoro-2-phenyl-2-propanol (HFPP), and 1,1,1,3,3,3-hexafluoro-2-(*p*-tolyl)-propanol (HFTP). It has been demonstrated that the degree of the broadening of the NIR absorption, which can be considered as a measure of polaron delocalization, depends strongly on the selection of an appropriate protonating agent−solvent couple. Several couples, giving spectra similar to that reported for PANI$(CSA)_{0.5}$ in *m*-cresol, have been found. Processing of PANI from HFIP solutions leads to films with improved PANI chains stacking order as evidenced by X-ray diffraction studies. The films exhibit metallic type of conductivity down to 200 K. The temperature dependence of the conductivity over the whole temperature range studied has been fitted using a combination of a metallic and hopping contribution in the frame of a heterogeneous disorder picture of PANI.

Introduction

Emeraldine salt—the only conductive form of polyaniline—has been extensively studied during the last 15 years mainly due to its interesting transport properties. Emeraldine salt is usually obtained from emeraldine base via protonation of its imine sites with a sufficiently strong acid:

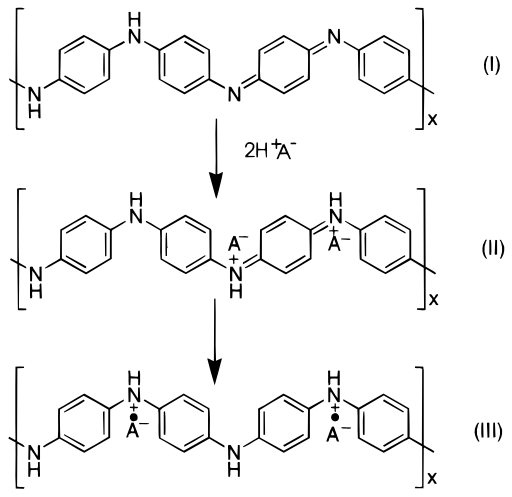

This protonation is accompanied by a charge redistribution (internal redox reaction) which leads to the formation of a polysemiquinone radical type of structure **III**, the so-called polaron lattice. The transformation of **II** into **III** renders all rings equivalent and strongly favors charge delocalization.

* To whom correspondence should be addressed.

Unfortunately, emeraldine (abbreviated as PANI) is extremely difficult to process, especially in its conductive form. This fact severely impedes its large scale technological applications. For this reason significant research effort has been directed, in the past few years, toward the improvement of solution and thermal processing of polyaniline.

In 1992 Cao et al.[1] demonstrated that the use of appropriately functionalized protonating agents induces solubility of conductive polyaniline. For example, the use of surfactant type protonating agents such as dodecylbenzenesulfonic acid facilitates the dissolution of protonated PANI in weakly polar solvents.[2] In selected cases, specific interactions between the functional groups of the doping anion and the solvent may induce conformational changes in the doped polymer which give rise to new, previously unobserved, properties of polyaniline both in solution and in the solid state. The most spectacular example of this type is the solubility inducing couple: *m*-cresol−camphorsulfonic acid (CSA). PANI$(CSA)_{0.5}$ solutions in *m*-cresol exhibit UV−vis−NIR spectra with a featureless absorption band increasing toward NIR, which is characteristic of charge delocalization.[3] Moreover, free-standing films of PANI$(CSA)_{0.5}$, cast from *m*-cresol solutions, show the highest conductivity of all types of nonoriented PANI films approaching, in selected cases, 400 $S \cdot cm^{-1}$.[1,2] These highly conductive films show several features characteristic of metallic behavior,[4] such as a negative dielectric constant in the low energy part, a Drude metallic response in the reflectance, temperature-independent Pauli-like susceptibility, and linear dependence of the thermoelectric power on temperature. The PANI−CSA/*m*-cresol (or other phenols of similar structure) system is not unique. It has been

S0024-9297(97)01365-X CCC: $15.00
Published on Web 04/11/1998

demonstrated that *m*-cresol solutions of PANI doped with such protonating agents as selected phosphonic acids or phosphoric acid diesters also give UV−vis−NIR spectra characteristic of delocalized charge.[5] Moreover *m*-cresol may be replaced by other solvents, for example 1,1,1,3,3,3-hexafluoro-2-propanol (HFIP).[6−7] $PANI(CSA)_{0.5}$ films processed from this solvent show conductivities comparable to those measured for $PANI(CSA)_{0.5}$ cast from *m*-cresol, i.e., between 100 and 400 $S{\cdot}cm^{-1}$.[1,2]

Similar to phenols, fluorinated alcohols are mildly acidic. In addition, they are good hydrogen-bonding donors. These two features should facilitate strong interactions of the solvent with polyaniline chains leading to conformational changes of the polymer and its solubility. Thus fluorinated alcohols are very good candidates for the use in solution processing of highly conducting PANI films. In this paper we investigate spectroscopic properties of basic and protonated polyaniline in HFIP and other fluorinated alcohols as well as structural and transport properties of free-standing films of conductive polyaniline prepared by casting from HFIP.

Experimental Section

Materials. Aniline 99% (Aldrich) was vacuum distilled prior to its use. Other chemicals were used without further purification. These were: ammonium persulfate 98% (Fluka), lithium chloride 99% (Aldrich), hydrochloric acid 37% aqueous solution (Carlo Erba), ammonia 25% aqueous solution (Prolabo), ethanol anhydrous (undenaturated) (Carlo Erba), chloroform 99% stabilized with 0.5−1% ethanol HPLC (Carlo Erba), 1-methyl-2-pyrrolidinone (NMP) 99% (Prolabo), *m*-cresol 99% (Merck), 1,1,1,3,3,3-hexafluoro-2-propanol (HFIP) 99% (Aldrich), 1,1,1,3,3,3-hexafluoro-2-phenyl-2-propanol (HFPP) (Fluorchem), 1,1,1,3,3,3-hexafluoro-2-(*p*-tolyl)-propanol (HFTP) (Fluorchem), 4,4′-biphenyl sulfonic acid (BP4S) 98% (Aldrich), bis(3-trifluoromethylbenzenesulfonyl imide) (TFMBSI) 98% (Fischer scientific), bis(perfluorobenzenesulfonyl imide) (PFBSI) 98% (Fischer scientific), dl-10-camphorsulfonic acid (CSA) 98% (Acros chemical), diisooctyl hydrogen phosphate (DiOHP) 97% (Aldrich), diphenyl hydrogen phosphate (DPHP) 99% (Acros chemical), 2-ketobutyric acid (KBuA) 99% (Aldrich), 1*H*,1*H*,2*H*,2*H*-perfluorooctanesulfonic acid (PFOSA) 99% (Fluorchem), phenol-4-sulfonic acid (PSA) 65 wt % in water (Fluka), phenylphosphonic acid (PPA) 98% (Acros chemical), pyruvic acid (PyA) 98% (Aldrich), and *p*-toluenesulfonic acid (TSA) 98% (Aldrich).

Preparation of PANI Solutions and Films. Oxidative polymerization of aniline was carried out at −26 °C in acidified water ethanol solution to which LiCl was added in order to increase the ionic strength of the reaction medium and to prevent the reaction mixture from freezing at the temperature of the polymerization. A 1:4 oxidant to aniline molar ratio was used. The temperature and the potential of the reaction mixture were monitored in situ during the polymerization using a 100 Ω Pt resistance thermometer and a reference electrode (SCE) which were connected to an automatic digital pH meter−mV meter (Schott CG841) controlled by a computer.[8]

In a typical preparation, 10 mL (0.1097 mol) of aniline was dissolved in 85 mL of 3 M aqueous solution of HCl to which 95 mL of ethanol and 16 g of LiCl were added. In a separate beaker 6.25 g (0.0274 mol) of ammonium persulfate was dissolved in 60 mL of 2 M aqueous solution of HCl containing 8 g of LiCl. Both solutions were cooled to −26 °C and mixed together. After ca. 65 min, when the potential of the reaction mixture dropped to ca. 540−560 mV vs SCE, the reactor was allowed to warm to room temperature. During the warming the potential dropped additionally to 440 mV vs SCE which is typical of emeraldine hydrochloride at room temperature. Then the precipitated polymer was separated on a Buchner funnel and repeatedly washed with 1 M HCl solution. The resulting emeraldine hydrochloride was dried to constant mass. Emeraldine hydrochloride was converted to emeraldine base by treatment with the excess of 0.1 M ammonia solution for 72 h. The powder of emeraldine base was then filtered, washed with water, and finally vacuum-dried to constant mass. Finally low molecular weight fraction was extracted with chloroform in a Soxhlet apparatus.

Emeraldine base used in further studies showed inherent viscosity of 2.31 $dL{\cdot}g^{-1}$. Inherent viscosity was determined at 25 °C on freshly prepared solutions using an Ubbelohde viscosimeter. 0.1 wt % PANI base solutions were prepared by stirring 36.7 mg of polymer powder in 20 mL of 96 wt % sulfuric acid for 15 h. The solutions were then filtered through a No. 4 frit prior to the measurements.

Both emeraldine base (PANI) and emeraldine protonated with camphorsulfonic acid ($PANI(CSA)_{0.5}$—where 0.5 denotes the number of acid molecules per repeat unit of PANI involving one ring and one nitrogen) readily dissolve in all three fluorinated solvents studied, i.e., 1,1,1,3,3,3-hexafluoro-2-propanol (HFIP), 1,1,1,3,3,3-hexafluoro-2-phenyl-2-propanol (HFPP), and 1,1,1,3,3,3-hexafluoro-2-(*p*-tolyl)-propanol (HFTP). The 0.5 wt % solutions of PANI or $PANI(CSA)_{0.5}$ were prepared by extending mixing of emeraldine base or CSA emeraldine salt at room temperature, followed by their filtration through a 0.2 μm fluoropolymer filter. Films were prepared by slow evaporation of the solvent—usually over 24−48 h. Solutions were cast on "inert" fluoropolymer substates. Due to the high volatility of HFIP, the casting of the films from this solvent was carried out in a small desiccator equipped with a Teflon stopcock which enabled periodical release of the overpressure.

Spectroscopic, Structural, and Transport Studies. Solution UV−vis−NIR spectra of PANI and $PANI(CSA)_{0.5}$ in fluorinated alcohols and the spectra of films cast from these solutions were measured on a CARY 2400 spectrometer.

Room-temperature EPR spectra of $PANI(CSA)_{0.5}$ films cast from HFIP were recorded on a BRUKER ER 200 EPR spectrometer.

X-ray diffraction studies were performed on a homemade three circles diffractometer equipped with a 1200 W power X-ray tube as a source of Cu Kα Ni-filtered radiation. The measurements were carried out in $\theta/2\theta$ transmission geometry using a point detector. The scan step was 0.05°, and the counting time was 45 s/step. Diffuse scattering from air was removed, and the data were corrected for absorption effects.

Absolute values of room-temperature conductivities of the films cast from HFIP were measured using a standard four-point method in Van der Pauw geometry.[9] Typical samples were square shaped (1 cm length), and their thicknesses were around 12−15 μm. The temperature dependence of the conductivity was measured on samples with four parallel line contacts. To ensure good electrical contacts, four gold lines were evaporated through a mask to which 25 μm golden wires were attached by pressing. The spacing between the contacts was ca. 1, 3, and 1 mm, and the sample width was around 2.5 mm. The temperature of the sample during the measurement was checked with a rhodium iron resistance thermometer which was placed in close proximity to the sample. To eliminate thermal gradients and other sources of errors, the conductivity was measured for both polarities and in each case the ohmic behavior was tested. The current was applied by a Keithley Model 220 current source, and the voltage was measured independently by two Keithley Model 6512 electrometers with an input impedance of 2×10^{14} Ω. The probe head was placed into a continuous flow helium cryostat allowing the conductivity measurements in the temperature range of 4−300 K.

Results and Discussion

Fluorinated alcohols readily dissolve PANI base giving solutions with distinctly different spectral features than those reported for other solvents. In Figure 1 PANI spectra in NMP, *m*-cresol and HFIP are compared. In nonprotonating solvents such as NMP, two

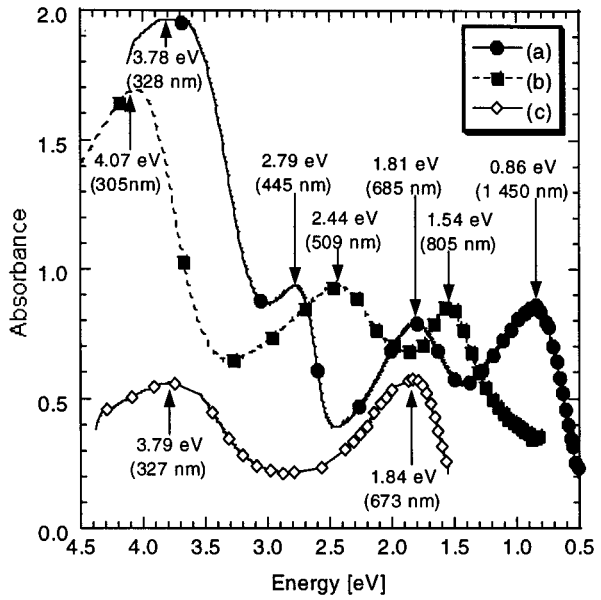

Figure 1. UV−vis−NIR spectra of PANI base in (a) MC solution, (b) HFIP solution, and (c) NMP solution.

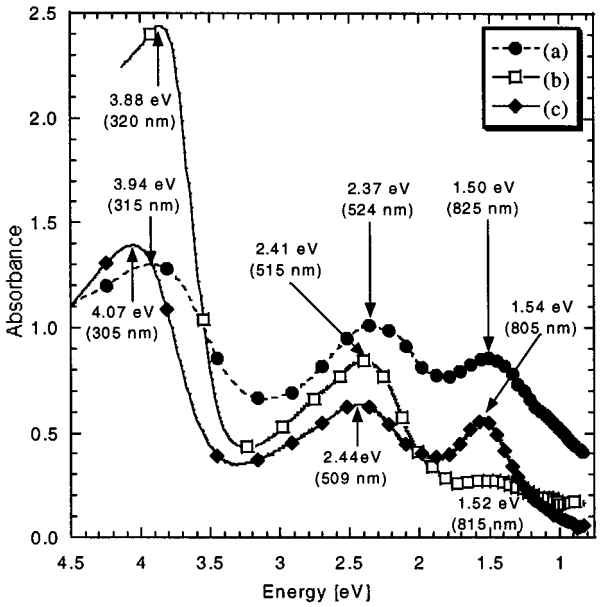

Figure 2. UV−vis−NIR spectra of PANI base in (a) HFPP solution, (b) HFTP solution, and (c) HFIP solution.

absorptions can be distinguished at 3.79 and 1.84 eV. The higher energetic absorption is ascribed to a $\pi-\pi^*$ transition in the benzoid ring whereas the lower energetic one to benzoid to quinoid ring excitonic transition. Thus the presence of two peaks in NMP solution of PANI base can be taken as a manifestation of the presence of two types of chemically nonequivalent rings in the polymer chain, namely the benzoid and the quinoid ones.

The spectrum of PANI base in *m*-cresol can be treated as a superposition of the spectrum of PANI base in NMP with the spectrum of protonated PANI. In addition to peaks characteristic of PANI base in NMP, two new peaks indicative of protonation can clearly be observed at 2.79 and 0.86 eV. This means that mildly acidic *m*-cresol at least partially protonates PANI.

Three distinct peaks are present in the spectrum of PANI base in HFIP—none of which coincides with the peaks registered for the NMP and *m*-cresol solutions of PANI. By analogy with NMP solutions, two peaks at higher energy (4.07 and 2.44 eV) can be explained as originating from the $\pi-\pi^*$ transition in the benzoid ring and the benzoid to quinoid ring excitonic transition, respectively. Experiments support this assignment. The peak at 4.07 eV is the only one that remains after the reduction of emeraldine base to leucoemeraldine;[10] thus, it must originate from the benzoid ring transition. The second peak at 2.44 eV decreases in intensity at the expense of the third peak (at 1.54 eV) after the addition to the solution of small amounts of protonating agents stronger than fluorinated alcohols.[10] Since the protonation involves the simultaneous disappearance of the quinoid sequence of the bonds, the second peak must correspond to the excitonic transition involving the quinoid ring. The same reasoning leads us to the conclusion that the third peak is due to the protonation of PANI base with HFIP. It should be noted that the use of HFIP as PANI base solvent induces significant blue shifts of all peaks with respect to the corresponding peaks recorded for NMP and *m*-cresol solutions. Strong interactions of the solvent with PANI base lead therefore to significant conformational changes in PANI chains favoring less conjugated structures.

PANI base solution in HFPP gives a spectrum similar to that recorded for the solution in HFIP (Figure 2). The maxima of three absorptions are however slightly red shifted with respect to the maxima recorded for HFIP solutions. Both HFIP ($pK_a = 9.3$)[11] and HFPP ($pK_a = 9.0$)[12] are slightly more acidic than *m*-cresol ($pK_a = 10.09$).[13] It is therefore reasonable to postulate that they protonate PANI base.

The spectrum of the solution of PANI base in HFTP is more different (Figure 2). First, it shows a much stronger $\pi-\pi^*$ absorption, which is only slightly (0.09 eV) blue shifted with respect to the correspondning absorptions in *m*-cresol and NMP solutions. In addition the protonation peak at 1.52 eV is very weak.

These spectral changes induced by the interactions of the solvent with PANI disappear after the removal of the solvent. For example UV−vis−NIR spectrum of a solid film cast from PANI−HFIP solution is essentially the same as the spectrum of a film cast from NMP and very similar to the solution spectrum of PANI in NMP.[10,14] Fluorinated alcohols, studied in this research, differ however in their volatility. In addition, in solutions with PANI base, their volatility is lowered due to the interactions with the polymer. Although HFIP (bp = 59 °C) can be totally removed upon casting,[14] in films cast from HFTP (bp = 181 °C) those alcohol molecules which protonate PANI base cannot be removed from the polymer matrix even after 18 h of heating under dynamic vacuum of 20 mmHg at 50 °C. The resulting spectrum of the film is similar to the spectrum of a PANI base−HFTP solution (compare parts a and b of Figure 3).

As has already been stated, the addition of small amounts of a protonating agent to a PANI base−fluorinated alcohol solution results in a decrease of the medium peak (in the vicinity of 2.40 eV) with a simultaneous growth and broadening of the low-energy peak around 1.50 eV. This asymmetric broadening extending to lower energies is better observed if the nanometer scale is used in the presentation of the UV−vis−NIR spectra instead of the eV scale. For this reason, in the UV−vis−NIR spectra of protonated PANI, the diagram abscissa is expressed in nanometers. If a

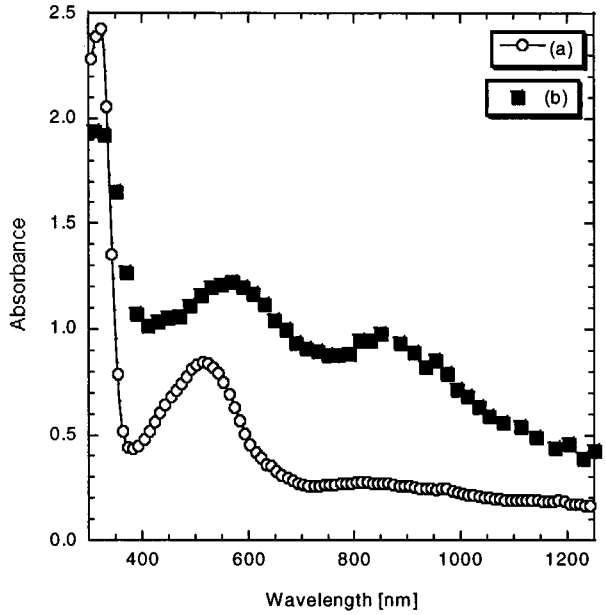

Figure 3. UV−vis−NIR spectra of (a) PANI base solution in HFTP and (b) PANI base film cast from HFTP solution.

sufficient amount of a protonating agent is added to the PANI base−fluorinated alcohol solution, to fully protonate all imine sites, i.e., for the composition of PANI-$(CSA)_{0.5}$, the absorption due to the protonation becomes very broad.

The problem of strong broadening of the NIR absorption, observed not only in fluorinated alcohol solvents but also for the solutions of protonated PANI in selected solvents of phenolic family, has been addressed by several authors. MacDiarmid et al.[15,16] introduced the term "secondary doping" to describe the interactions of *m*-cresol and other phenols with protonated PANI. In particular, in ref 3, they described two types of PANI-$(CSA)_{0.5}$ spectra. In inert solvents a narrow absorption peak in the vicinity of 800 nm is observed, whereas in solvents strongly interacting with protonated PANI a featureless increase of absorption extending toward the NIR is recorded. This absorption tail is characteristic of polaron delocalization.

In a series of papers Ikkala et al.[17−19] used the concepts of supramolecular chemistry in the explanation of spectral features of sulfonic acid protonated PANI in phenol type solvents. Thus, the formation of extended chain conformation in protonated PANI which, in turn, favors polaron delocalization, requires strong interactions via hydrogen bonding between the solvent, the counteranion, and the polymer chain, together with a geometrical match between the solvent and polymer repeat units in order to enhance the van der Waals interaction. This is an attractive concept because it implies that polaron delocalization in PANI can be obtained for counterion−solvent couples which differ significantly in chemical nature from sulfonic acid anions and phenols, provided that the molecules involved are capable of interacting via hydrogen bonding and the geometrical match conditions are fulfilled. Moreover the degree of polaron delocalization will depend on the degree of steric matching between the solvent and PANI repeat unit. Thus, NIR absorption bands differing in the extent of their delocalization can be obtained for PANI protonated with the same acid but dissolved in different solvents of the same family. This

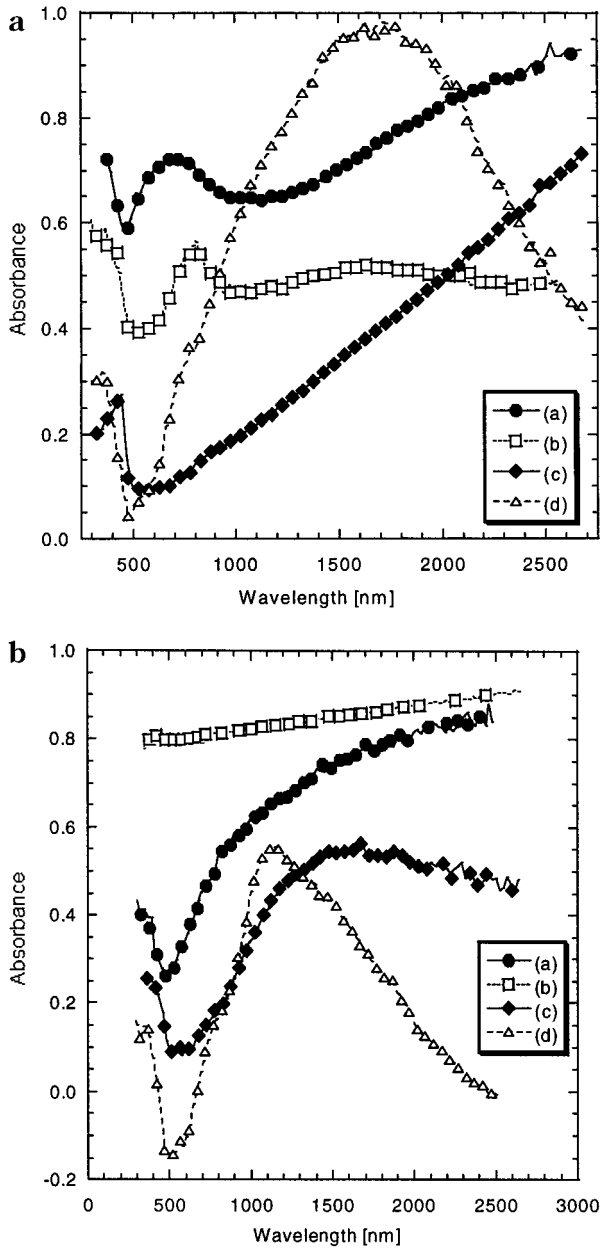

Figure 4. (a) UV−vis−NIR spectra of PANI−CSA in (a) HFTP solution, (b) HFPP solution, (c) MC solution, and (d) HFIP solution. (b) UV−vis−NIR spectra of PANI−PSA in (a) HFTP solution, (b) HFPP solution, (c) MC solution, and (d) HFIP solution.

is clearly manifested for PANI$(CSA)_{0.5}$ and PANI-$(PSA)_{0.5}$ (where PSA = phenol-4-sulfonic acid) (parts a and b of Figure 4).

PANI$(CSA)_{0.5}$ in HFIP gives a broad NIR peak with a maximum at 1750 nm. The replacement of hydrogen at C(2) of HFIP by phenyl ring induces further broadening. In HFPP solution of PANI$(CSA)_{0.5}$ the NIR absorption is very broad, but the maximum around 1750 nm is still visible. In addition a narrow absorption peak with a maximum around 800 nm is superimposed on the delocalized one. For HFTP solutions, the NIR absorption increases monotonically, and no maximum can be observed up to 2600 nm. In the case of PANI-$(CSA)_{0.5}$, none of the solvents of the family of fluorinated alcohols gives as clear an NIR tail as *m*-cresol does. However a change in the protonating agent from CSA to PSA significantly alters the picture.

Table 1. UV−Vis−NIR Characterization of Protonated PANI Solutions in Phenolic and Fluorinated Solvents[a]

	MC Phenolic solvent		HFIP Fluorinated solvent		HFPP Fluorinated solvent		HFTP Fluorinated solvent	
CSA	Delocalized		Broadened		Mixed		Mixed	
	448 nm NIR tail till 2 700 nm	2.77 eV NIR tail till 0.46 eV	440 nm 1 700 nm	2.81 eV 0.73 eV	440 nm 790 nm 1 680 nm	2.82 eV 1.57 eV 0.74 eV	440 nm 710 nm NIR tail till 2 700 nm	2.82 eV 1.75 eV NIR tail till 0.46 eV
PSA	Broadened		Broadened		Delocalized		Delocalized	
	380 nm 1 625 nm	3.26 eV 0.76 eV	444 nm 1 150 nm	2.79 ev 1.08 eV	443 nm NIR tail till 2 700 nm	2.80 eV NIR tail till 0.46 eV	415 nm NIR tail till 2 700 nm	2.99 eV NIR tail till 0.46 eV
TSA	Delocalized						Delocalized	
	444 nm NIR tail till 2 500 nm	2.79 eV NIR tail till 0.50 eV					410 nm NIR tail till 2 700 nm	3.02 eV NIR tail till 0.46 eV
BP4S	Delocalized						Mixed	
	444 nm NIR tail till 2 500 nm	2.79 eV NIR tail till 0.50 eV					410 nm 780 nm NIR tail till 2 500 nm	3.02 eV 1.59 eV NIR tail till 0.50 eV
PFOSA	Broadened		Broadened				Delocalized	
	439 nm 1 875 nm	2.82 ev 0.66 eV	440 nm 1 750 nm	2.82 ev 0.71 eV			405 nm NIR tail till 2 700 nm	3.06 eV NIR tail till 0.46 eV
PPA	Mixed		Delocalized		Mixed		Mixed	
	437 nm 900 nm NIR tail till 2 200 nm	2.84 eV 1.38 eV NIR tail till 0.56 eV	439 nm NIR tail till 2 700 nm	2.82 eV NIR tail till 0.46 eV	440 nm 790 nm 1 800 nm	2.82 eV 1.57 eV 0.69 eV	440 nm 800 nm 1 650 nm	2.82 eV 1.55 eV 0.75 eV
DiOHP	Mixed		Mixed					
	444 nm 900 nm NIR tail till 2 000 nm	2.79 eV 1.38 eV NIR tail till 0.62 eV	425 nm 855 nm 1 185 nm	2.92 eV 1.45 eV 1.05 eV				
DPHP			Mixed					
			420 nm 825 nm 1 160 nm	2.95 eV 1.50 eV 1.07 eV				
TFMBSI			Mixed					
			420 nm 800 nm 1 500 nm	2.95 eV 1.55 eV 0.83 eV				
PFBSI			Mixed					
			420 nm 800 nm 1 100 nm	2.95 eV 1.55 eV 1.13 eV				
PyA	Mixed		Broadened				Localized	
	425 nm 935 nm 2 200 nm	2.92 eV 1.33 eV 0.56 eV	420 nm 1 070 nm	2.95 ev 1.16 eV			420 nm 835 nm	2.95 eV 1.48 eV
KBuA	Mixed		Broadened				Localized	
	425 nm 945 nm NIR tail till 2 700 nm	2.92 eV 1.31 eV NIR tail till 0.46 eV	420 nm 1 030 nm	2.95 ev 1.20 eV			420 nm 825 nm	2.95 eV 1.50 eV

[a] Types of NIR bands: (1) monotonic increase without a maximum termed as "Delocalized"; (2) broad band over several hundreds of nm showing a maximum termed as "Broadened"; (3) localized with a clear maximum in the vincinity of 800−1000 nm termed as "Localized"; (4) Superposition of spectral features of (1) and (3) or (2) and (3) termed as "Mixed".

As in the case of PANI$(CSA)_{0.5}$, PANI$(PSA)_{0.5}$ in HFIP gives a broad NIR peak with a clear maximum. This peak further broadens for HFPP solvent and for HFTP the absorbance increases monotonically as in the case of PANI$(CSA)_{0.5}$ in *m*-cresol. On the contrary PANI-$(PSA)_{0.5}$ in *m*-cresol gives clear NIR absorption peak with the maximum around 1700 nm.

Thus, the degree of the delocalization of polarons, as manifested by the changes in the NIR absorption band for PANI doped with a given counterion, can be altered by changing the steric interactions between the solvent and the protonated PANI chain. In Table 1, we collected spectral characteristics of protonated PANI solutions of all PANI counterion−solvent couples tested in this research.

The next question to be answered is the influence of the solvent on the UV−Vis−NIR spectra of the resulting films obtained after the evaporation of the solvent. Two cases must be considered. Low-volatile, strongly interacting with protonated PANI solvents cannot be totally removed from the solid polymer matrix even after extending drying in dynamic vacuum. Wide-angle X-ray

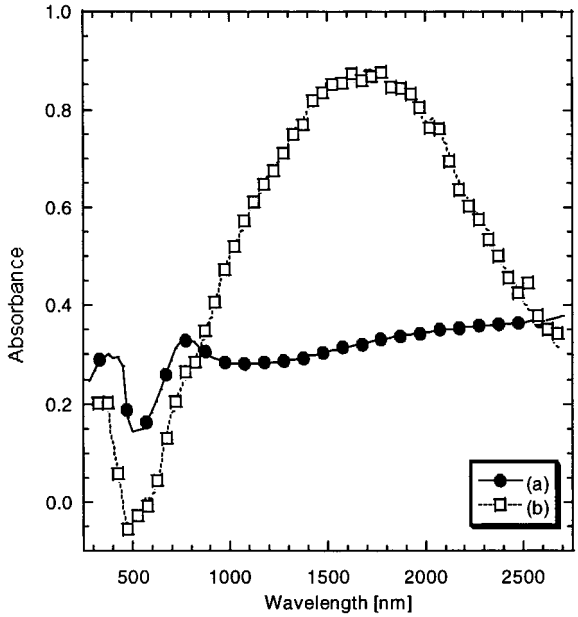

Figure 5. UV−vis−NIR spectra of (a) PANI−CSA thin film (No residual HFIP) and (b) PANI−CSA solution in HFIP.

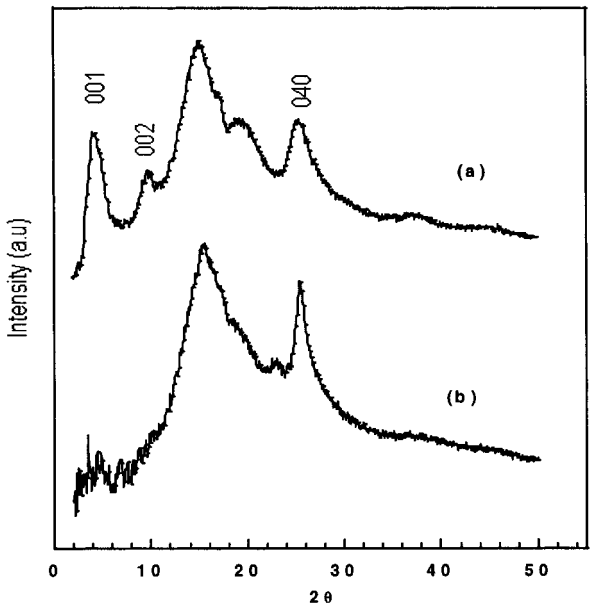

Figure 6. Wide angle X-ray diffraction profiles of (a) PANI−CSA film cast from *m*-cresol and (b) PANI−CSA film cast from HFIP. The indexation of indicated lines corresponds to the monoclinic unit cell model described in ref 20 (see text). The profiles are shifted for more clarity.

scattering (WAXS) data obtained for PANI(CSA)$_{0.5}$ cast from *m*-cresol indicate that the remaining solvent does not enter the crystalline regions of the polymer but it instead stays in its amorphous parts. Ikkala et al.[17,18] postulated that *m*-cresol present in the amorphous domains strongly influences the packing in solvent-free crystalline PANI(CSA)$_{0.5}$ regions. According to these authors high, metallic type conductivity in PANI(CSA)$_{0.5}$ is achieved due to the combination of the layered structure of the solvent molecules coplanar with the PANI rings and stacking effects.

Are small amounts of solvent and solvent/polymer phenyl ring/phenylene ring stackings really necessary to achieve metallic conductivity in PANI(CSA)$_{0.5}$? To verify this hypothesis we have studied the films cast from HFIP. This solvent, which shows an acidity and a hydrogen bonding formation capability similar to those of *m*-cresol, has no aromatic ring in its structure. In addition it can be efficiently removed from the polymer matrix since elemental analysis of PANI(CSA)$_{0.5}$ films cast from HFIP shows a negligible amount of fluorine.[6,14] In Figure 5, solution spectrum of PANI(CSA)$_{0.5}$ in HFIP is compared with spectrum of the same PANI(CSA)$_{0.5}$ after the evaporation of the solvent. The solution and solid state spectra differ significantly in this case. Upon removal of the solvent the NIR absorption band gradually evolves to a monotonically increasing NIR absorption tail. However a small contribution of the localized states is observed around 750−800 nm. This band is also observed in the solution spectra as a shoulder of the intense broad NIR absorption with the maximum at 1700 nm.

The improvement in the polaron band delocalization implies that, upon casting, a more planar conformation of PANI chains is achieved in PANI(CSA)$_{0.5}$ processed from HFIP solution which facilitates the formation of crystalline domains and leads to high conductivity possibly of metallic type. Both hypotheses have been confirmed by experiments.

Indeed, PANI(CSA)$_{0.5}$ obtained by casting from HFIP shows a relatively high degree of crystallinity of ca. 20% as estimated from the ratio of the integrated intensity of the reflections corresponding to the crystalline phase to the total integrated intensity. In Figure 6 a typical diffractogram of PANI(CSA)$_{0.5}$ processed from HFIP is compared with that of PANI(CSA)$_{0.5}$ cast from *m*-cresol. Both diffractograms were obtained under identical experimental conditions.

Before discussing the differences between both X-ray diffraction patterns, it is instructive to briefly describe the structural models elaborated for CSA protonated polyaniline.[20] In the proposed two models, crystalline structure of PANI(CSA)$_{0.5}$ can be described either by a monoclinic unit cell (a = 6.9 Å, b = 13.8 Å, c = 21.5 Å, β = 120°) or by a triclinic one (a = 13.8 Å, b = 8.5 Å, c = 21.5 Å, α = 105°, β = 114°, γ = 155°). These two models are very close and can be considered as lamellar structures in which flat polymer chains alternate with layers of anions originating from a CSA dopant. One main difference between the two models is the exact position of dopant anions with respect to the PANI chains. It turned out during the computer modeling of the structure that relative intensities of Bragg reflections were strongly influenced by the changes in the conformation of the dopant anions and their orientation with respect to the PANI chains. On the contrary, the exact conformation of PANI chains infuences the X-ray diffraction pattern to a much lesser extent.

The main differences between the diffractogram of PANI(CSA)$_{0.5}$ cast from *m*-cresol and that of PANI(CSA)$_{0.5}$ cast from HFIP can be described as follows. In the polymer obtained from the fluorinated alcohol solution there exists a distinct peak at 2θ = 25°, which is more intense and narrower than the corresponding peak in the X-ray pattern of the film processed from *m*-cresol. According to the developed models this reflection corresponds to the periodicity in the chain−ion−chain stacking direction and is indexed as 040 in the monoclinic cell. The above observation suggests therefore more ordered stacking and a larger coherence length in the chain stacking direction in PANI(CSA)$_{0.5}$ prepared from the HFIP solution. However, crystalline

order along the chain axis seems at first glance to be worse than in the case of the film processed from *m*-cresol. Indeed, in the diffraction pattern of the latter the reflections corresponding to the periodicities along the chains (00*l* lines) are clearly resolved (reflections at $2\theta = 4.2$ and 9.6°) whereas in the HFIP originating film they are broad and very weak.

At this point, it should be noted that the diffractogram of PANI(CSA)$_{0.5}$ reported in this research is different not only from that recorded for the *m*-cresol processed film but also from the diffractogram reported by Hopkins et al.[6,14] for PANI(CSA)$_{0.5}$ cast from HFIP. A strong 001 peak at ca. 4.5° is clearly visible in the X-ray pattern reported by Hopkins et al. On the contrary the peak at 25° present in our diffractograms is nonexistent in the diffractogram reported by Hopkins et al.

The most plausible explanation of this effect involves a "texture" effect. In such a case the relative intensities of particular Bragg reflections should depend on the diffraction geometry. Indeed, our data were obtained from the transmission geometry whereas Hopkins et al.[6,14] used the reflection geometry.[21] According to ref 20, that would mean the long chain axis direction is isotropically distributed in the plane of the films cast from *m*-cresol while it is not the case for films cast from HFIP. In other words, films cast from *m*-cresol can be considered as 2D in-plane powders but not in their thickness, as shown in ref 22, while films from HFIP seem to exhibit more pronouced in-plane and out-of-plane anisotropies. More detailed studies of the texture in PANI(CSA)$_{0.5}$ are in progress.

At this stage of the study, it clearly appears that the solvent is definitively not a component of the crystalline structure in CSA-protonated PANI. Due to the high volatility of HFIP, the films obtained by casting are free of solvent as confirmed by mass changes and elemental analysis.[6,14] From a structural point of view, our results and those published previously[23] show that HFIP cast films are isomorphous with those processed from *m*-cresol. Since *m*-cresol cast films contain 10−15 wt % of the solvent, the data presented here unequivocally show that *m*-cresol remains in the amorphous parts of the film.

The high conductivity of PANI(CSA)$_{0.5}$ films processed from HFIP is strongly manifested in EPR spectra of this polymer. Even for relatively thin samples (12−15 μm), a highly asymmetric Dysonian line shape is observed which is indicative of the "skin effect" frequently observed in materials with sufficiently high conductivity.

To verify whether PANI(CSA)$_{0.5}$ films processed from HFIP exhibit the metallic type of conductivity, we have studied the temperature dependence of the conductivity of these films. Such studies require careful removal of water adsorbed on the sample. It is known[24] that adsorbed water increases the electronic conductivity of PANI. Thus, its incomplete removal might result in a false temperature characteristic of the conductivity. To eliminate the influence of adsorbed water, we have pumped the sample in the cryostat for ca. 1 h prior to the onset of the temperature lowering. During the first 10 min of pumping a fast decrease of the conductivity was observed due to outgoing water, and then after an additional 45−50 min, the conductivity nearly stabilized.

In Figure 7 the temperature dependence of the conductivity of two PANI(CSA)$_{0.5}$ films, showing the highest room temperature (RT) conductivity, is presented in a linear scale. The measured RT conductivity is within the range of 200−270 S·cm^{-1}, the value comparable to Mott's minimum metallic conductivity.[25] Despite the fact that the absolute value of the RT conductivity of film 2 is lower than in the case of film 1, its metallic character ($d\sigma/dT < 0$) persists down to 200 K whereas for film 2 the maximum of the conductivity is observed at 220 K.

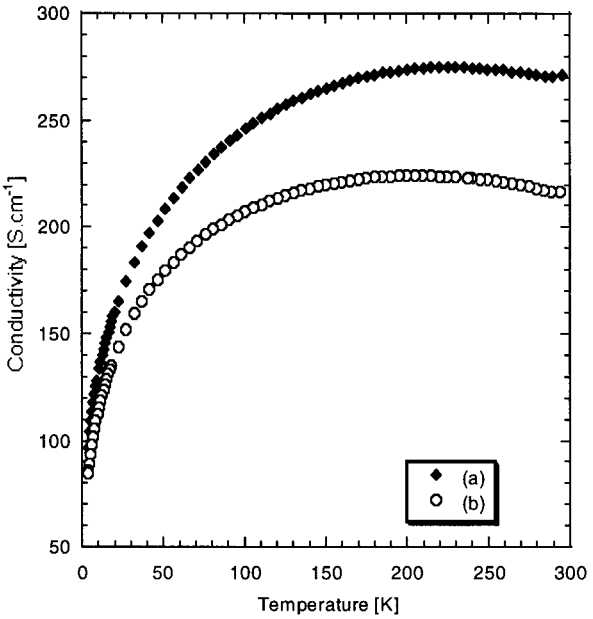

Figure 7. Linear plot of the conductivity vs temperature for two different PANI−CSA films cast from HFIP solution: (a) film 2; (b) film 1.

In this temperature range the conductivity shows a negative temperature coefficient, as in a true metal. For lower temperatures the conductivity decreases and a simple extrapolation shows a vanishing conductivity for $T = 0$, indicating insulating behavior for low temperatures.

Another method to look more carefully to the physical state of PANI(CSA)$_{0.5}$ films is to calculate and plot the reduced activation energy $W(T)$, which is defined as:

$$W(T) = T\, d[\ln \sigma(T)]/dT \qquad (1)$$

and plot it vs temperature. This type of plot allows one to distinguish between the three following states of a metal−insulator (MI) phase transition:

(i) the metallic behavior, which is signified by a negative slope, (ii) the semiconducting behavior, showing a positive slope; and (iii) the critical regime, characterized by a horizontal line for lower temperatures.

The MI transition occurs when the disorder is sufficiently weak. In this case the mobility edges move away from the center of the band toward the band tails such that the Fermi level (E_F) lies in the region of extended states. The temperature dependence of $W(T)$ of PANI(CSA)$_{0.5}$ films cast from HFIP is shown in Figure 8. As at lower temperatures $W(T)$ vs T gives a horizontal line, it can be concluded that the films can be characterized as being in the critical regime of the MI transition.

For heavily doped conducting polymers the model of Sheng[26] has been widely applied, but this model cannot explain the characteristics of PANI(CSA)$_{0.5}$ films cast from HFIP. In the frame of a heterogeneous disorder

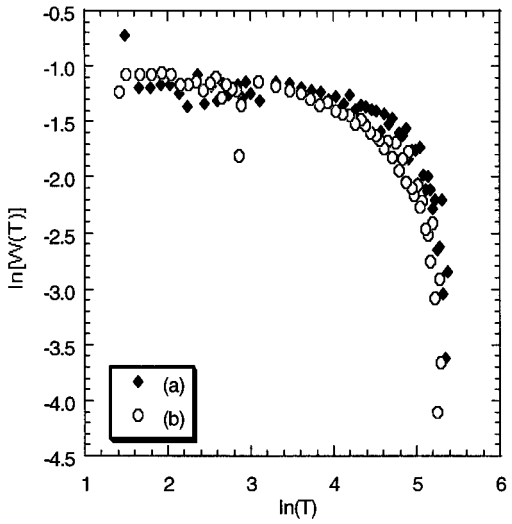

Figure 8. Logarithmic plot of the reduced activation energy $W(T)$ vs $\ln(T)$ for two different PANI−CSA films cast from HFIP solution: (a) film 2; (b) film 1. The shape of the curve in this plot determines the physical state of samples. The horizontal line observed in the low-temperature range indicates that the polymer studied is in the critical regime of a MI transition.

picture, we have used a combination of a metallic and a hopping contribution to the conductivity in order to describe the temperature dependence of conductivity in the whole temperature range studied.[27−29]

The high-temperature part, i.e., the part above the maximum of the conductivity, is dominated by quasi-1D metallic conduction along polymer chains which is proportional to $\exp(\hbar\omega/T)$.[30]

For the low-temperature description of the critical regime of the MI transition, Larkin and Khmel'nitskii[31] found that the resistivity is not activated, but follows a power law as a function of temperature

$$\sigma(T) = (e^2 p_F/\hbar^2)(k_B T/E_F)^{1/\eta} \sim T^b \qquad (2)$$

where p_F is the Fermi momentum and e the electron charge. η is typically between 1 and 3.[31]

To account for the experimental data, we used the expression

$$\sigma^{-1} = \rho = \rho_1 * T^{-b} + \rho_2 * \exp(-\hbar\omega/kT) \qquad (3)$$

where ρ_1, ρ_2, b, and $\hbar\omega$ are constants. The first term describes the hopping process whereas the second one corresponds to the metallic behavior. For the typical phonon frequency of $\hbar\omega/k = 500$ K we get a good agreement between the calculated conductivities and the experimental data. In Figure 9 the experimental results are compared with the calculated curves. The fit parameters obtained for film 1 and film 2 are collected in Table 2. The obtained good fit indicates that the conductivity follows the power-law behavior in the temperature range below 100 K and the quasi-1D metallic behavior around RT.

This change of behavior from metallic to insulating can be explained by a transition from a phonon-controlled metallic state at RT to a nonmetallic state with localized carriers and hopping transport in the low-temperature range.[32]

Conclusions

In brief, we have studied spectrosopic features of polyaniline base solutions in selected fluorinated alcohols as well as the solutions of strong acids protonated polyaniline in these solvents. We have demonstrated by UV−vis−NIR that the degree of polaron delocalization can be adjusted by the selection of an appropriate protonating agent-solvent couples. By processing PANI-$(CSA)_{0.5}$ from 1,1,1,3,3,3-hexafluoro-2-propanol, we have obtained films exhibiting improved chain stacking order and metallic character of conductivity down to 200 K.

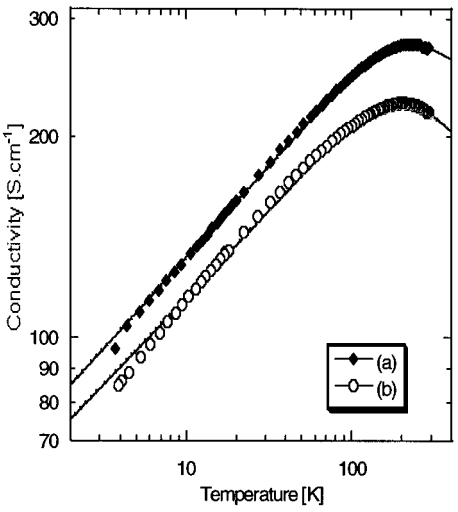

Figure 9. Log−log plot of conductivity σ ($S\cdot cm^{-1}$) vs temperature for two different PANI−CSA films cast from HFIP solution: (a) film 2; (b) film 1. The shape of the curve in this plot shows that experimental data follow a power law behavior over a wide temperature range. The full line corresponds to a fit of experimental data with eq 3.

Table 2. Fitting Parameters of eq 3 Obtained for PANI$(CSA)_{0.5}$ Films

	ρ_1	ρ_2	b
film 1	0.0155	0.00475	0.239
film 2	0.0142	0.00374	0.273

Acknowledgment. We want to acknowledge financial contributions of the Agence Rhône-Alpes pour la Maîtrise des Matériaux funding through the "Polymères Conducteurs Electronique" research programm.

References and Notes

(1) Cao, Y.; Smith, P.; Heeger, A. J. *Synth. Met.* **1992**, *48*, 91−97.
(2) Cao, Y.; Qiu, J.; Heeger, A. J. *Synth. Met.* **1995**, *69*, 187−190.
(3) Xia, Y.; Wiesinger, J. M.; MacDiarmid, A. G. *Chem. Mater.* **1995**, *7*, 443−445.
(4) Kohlman, R. S.; Joo, J.; Epstein, A. J. In *Physical Properties of Polymers Handbook*; Mark, J. E., Ed.; AIP Press: Woodbury, NY, 1996; Chapter 34, p 453.
(5) Pron, A.; Nicolau, Y. F.; Genoud, F.; Nechtschein, M. *J. Appl. Polym. Sci.* **1997**, *63*, 971− 977.
(6) Hopkins, A. R.; Rasmussen, P. G.; Basheer, R. A. *Macromolecules* **1996**, *29*, 7838−7846.
(7) Carter, S. A.; Angelopoulos, M.; Karg, S.; Brock, P. J.; Scott, J. C. *Appl. Phys. Lett.* **1997**, *70*, 2067−2069.
(8) Beadle, P. M.; Nicolau, Y. F.; Banka, E.; Rannou, P.; Djurado, D. *Synth. Met.*, in press.
(9) Montgomery, H. C. *J. Appl. Phys.* **1971**, *42*, 2971−2975.
(10) Kulszewicz-Bajer, I.; Wielgus, I.; Pron, A.; Rannou, *Macromolecules* **1997**, *30*, 7091−7095.
(11) Sheppard, W. A.; Sharts, C. M. In *Organic Fluorine Chemistry*; W. A. Benjamin Inc.: New York, 1969; p 436.
(12) Filler, R. In *Fluorine Chemistry Reviews*, Tarrant, P., Ed.; Marcel Dekker Inc.: New York, 1977; p 6.

(13) *Techniques of Chemistry*, 4th ed.; Riddick, J. A., Bunger, W. B., Sakano, T. K., Eds.; Wiley-Interscience: New York, 1986; Vol II, Chapter 1, p 247.
(14) Hopkins, A. R.; Rasmussen, P. G.; Basheer, R. A. *Polym. Prepr.* **1995**, *36*, 396−397.
(15) MacDiarmid, A. G.; Epstein, A. J. *Synth. Met.* **1994**, *65*, 103−116.
(16) MacDiarmid, A. G.; Epstein, A. J. *Synth. Met.* **1995**, *69*, 85−92.
(17) Ikkala, O. T.; Pietilä, L.-O.; Ahjopalo, L.; Österholm, H.; Passiniemi, P. J. *J. Chem. Phys.* **1995**, *103*, 9855−9863.
(18) Vikki, T.; Pietilä, L.-O.; Österholm, H.; Ahjopalo, L.; Takkala, A.; Toivo, A.; Levon, K.; Passiniemi, P.; Ikkala, O. *Macromolecules* **1996**, *29*, 2945−2953.
(19) Ikkala, O. T.; Pietilä, L.-O.; Passiniemi, P.; Vikki, T.; Österholm, H.; Ahjopalo, L.; Österholm, J.-E. *Synth. Met.* **1997**, *84*, 55−59.
(20) Luzny, W.; Samuelsen, E. J.; Djurado, D.; Nicolau, Y. F. *Synth. Met.* **1997**, *90*, 19−23.
(21) Hopkins, A. R. Personal communication to P. Rannou, 1997.
(22) Minto, C. D. G.; Vaughan, A. S. *Polymer* **1997**, *38*, 2683−2688.
(23) Djurado, D.; Nicolau, Y. F.; Dalsseg, I.; Samuelsen, E. J. *Synth. Met.* **1997**, *84*, 121−122.
(24) Travers, J. P.; Nechtschein, M. *Synth. Met.* **1987**, *21*, 135−141.
(25) Reghu, M.; Cao, Y.; Moses, D.; Heeger, A. J. *Phys. Rev. B* **1993**, *47*, 1758−1764.
(26) Sheng, P.; Klafter, J. *Phys. Rev. B* **1983**, *27*, 2583−2586.
(27) Kohlman, R. S.; Tanner, D. B.; Ihas, G. G.; Min, Y. G.; MacDiarmid, A. G.; Epstein, A. J. *Synth. Met.* **1997**, *84*, 709−714.
(28) Kaiser, A. B. *Phys. Rev. B* **1989**, *40*, 2806−2813.
(29) Kaiser, A. B.; Liu, C.-J.; Guilbert, P. W.; Chapman, B.; Kemp, N. T.; Wessling, B.; Partridge, A. C.; Smith, W. T.; Shapiro, J. S. *Synth. Met.* **1997**, *84*, 699−702.
(30) Kivelson, S.; Heeger, A. J. *Synth. Met.* **1990**, *22*, 371−384.
(31) Larkin, A. I.; Khmel′nitskii, D. E. *Sov. Phys. JETP* **1982**, *56*, 647−652.
(32) Joo, J.; Prigodin, V. N.; Min, Y. G.; MacDiarmid, A. G.; Epstein, A. J. *Phys. Rev. B* **1994**, *50*, 12226−12229.

MA971365F